



# Estimation of the share of artificial Po-210 contamination in the ambient air

Magdalena Długosz-Lisiecka\*, Karolina Nowak

Lodz University of Technology, Institute of Applied Radiation Chemistry, Łódź, Poland

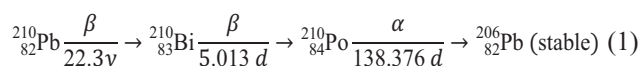
\*Corresponding author's e-mail: [mdlugosz@mitr.p.lodz.pl](mailto:mdlugosz@mitr.p.lodz.pl)

**Keywords:** source apportionment, radioactive aerosols, unsupported  $^{210}\text{Po}$

**Abstract:** In this work, source apportionment for unsupported  $^{210}\text{Po}$  was conducted. The activity size distributions of both supported and unsupported  $^{210}\text{Po}$  in urban aerosols were measured from February to December 2019. The results confirmed that the activity of  $^{210}\text{Po}$  in the atmosphere is significantly increased by additional  $^{210}\text{Po}$  content related to coal combustion by-product releases, especially in the cold winter season. The sources of this content are local emissions and long-range transport processes. Unsupported activity concentrations of  $^{210}\text{Po}$  and weather parameters (temperature, humidity, and wind velocity) were used for source apportionment from three heating systems.

## Introduction

Radon isotopes exhaled from the ground surface are diffused and advected into the atmosphere. Therefore, the  $^{222}\text{Rn}$  (half-life 3.8 days) isotope decay products of  $^{210}\text{Pb}$  (half-life 22 years),  $^{210}\text{Bi}$  (half-life 5 days) and  $^{210}\text{Po}$  (half-life 138 days) are widely used as tracers of various atmospheric processes. These radionuclides turn into radioactive aerosols through gas-particle conversion and coagulation.  $^{210}\text{Pb}$ ,  $^{210}\text{Bi}$  and  $^{210}\text{Po}$  isotopes attach to aerosol particles and reside in the atmosphere, and are then removed from the atmosphere through wet and dry deposition.



The  $^{210}\text{Pb}$ ,  $^{210}\text{Bi}$  and  $^{210}\text{Po}$  family connections and chemical properties cause similar behavior for all three isotopes in the fresh air. They are all involved in the condensation and coagulation processes of particles suspended in the atmosphere (Baskaran 2011). The activity concentrations (activity of isotope related to the mass of the sample) of the  $^{210}\text{Pb}$  decay products  $^{210}\text{Bi}$  and  $^{210}\text{Po}$  increase according to the age of the aerosols. Therefore, the well-known chronometer tool, aerosol residence time, is used to calculate the activity ratios.

The activity size distributions of  $^{210}\text{Pb}$ ,  $^{210}\text{Bi}$  and  $^{210}\text{Po}$  in the air change widely due to the geological structure of the region, source pollution apportionment,  $^{222}\text{Rn}$  exhalation and weather conditions (Ioannidou et al. 2019, Mertens et al. 2020, Phamet et al. 2011, Sýkora and Povinec 2020, Szaciłowski et al. 2019). Weather conditions strongly influence the fate of airborne radionuclides suspended in the atmosphere and  $^{222}\text{Rn}$  exhalation from the ground. The dynamics of isotope

production from  $^{222}\text{Rn}$  decay, weather changes and the presence of additional  $^{210}\text{Po}$  isotopes from natural or artificial sources mean that the measured values of  $^{210}\text{Po}$  in the air can change seasonally. Long-term measurements of airborne  $^{210}\text{Pb}$  isotopes show that they reach maximum concentration in the cold winter season and minimum concentration in the hot summer season (Długosz-Lisiecka 2016).

Higher natural  $^{210}\text{Po}$  content can be the result of  $^{210}\text{Bi}$  decay in a stable, poorly mixed atmosphere that supports the suspension of aerosols for a longer time. Higher dynamics of the atmosphere (high temperature and strong winds) dilute the long-lived  $^{222}\text{Rn}$  exhalation products. This effectively elutes the isotopes from the atmosphere and shortens the aerosol residence time. Different meteorological conditions influence the activity size distribution of radioactive aerosols (Ioannidou et al. 2019, Pham et al. 2011). A previous study based on the aerosol residence time calculated by two independent methods allowed the excess of  $^{210}\text{Po}$  activity concentration to be appraised (Długosz-Lisiecka 2015a,b, Długosz-Lisiecka 2016, Długosz-Lisiecka and Bem 2020, Vecchi et al. 2019).

The additional  $^{210}\text{Po}$  contribution does not come from the parent  $^{210}\text{Bi}$  present in existing aerosols; therefore, in the literature, this contribution has been named 'unsupported'  $^{210}\text{Po}$ . The relatively higher unsupported  $^{210}\text{Po}$  content in relation to natural, supported  $^{210}\text{Po}$  (built up from  $^{210}\text{Bi}$  decay) indicates the existence of a significant additional source of  $^{210}\text{Po}$  injection into the atmosphere. Many studies have confirmed the contribution of anthropogenic  $^{210}\text{Po}$  in the atmosphere and have identified the direct source. As a result,  $^{210}\text{Po}$  has become a tracer of combustion products (Ozden et al. 2016, 2017, Vaasma et al. 2017, Carvalho et al. 2017, Nelson et al. 2017).

Combusted fossil fuels release various types of pollutants and isotopes into the atmosphere, depending on the origin and

type of fuel used (Długosz-Lisiecka 2019, Wasielewski et al. 2020). The concentration of emitted radionuclides depends on their content in coal, the method and temperature of combustion, and the efficiency of fly ash recovery. Electrostatic precipitators do not capture fine particles, thus nanometer particles can escape freely into the atmosphere. Many studies confirm the increased activity of natural radionuclides near coal power plants (Behbehani et al. 2020, Aba et al. 2020, Ouyang et al. 2018, Yan et al. 2012, Wasilewski et al. 2020). In Romania, around 5 km from a power plant, the concentrations of some natural isotopes were 20% higher in the upper soil layer compared to deeper layers (Botezatu et al. 1996).  $^{210}\text{Pb}$  and  $^{210}\text{Po}$  are considered natural radionuclides. Their highest emission rates come from fossil fuel power plants, and they possess elevated potential radiation exposure risks to humans and the environment. Several studies confirm the highest activity concentration values of both isotopes in fine ash fractions, especially in fractions below  $2.5\ \mu\text{m}$  (Vaasma et al. 2017, Długosz-Lisiecka 2016, 2020, Marley et al. 2000, Yan et al. 2012, Filizok and Uğur 2019, Sabuti et al. 2011, 2013, Ouyang et al. 2019, Kaynar et al. 2018, Poluszyńska 2020).

In the climate of central Poland, the primary source of unsupported  $^{210}\text{Po}$  is the burning of coal for energy production. The Polish energy sector is based on hard coal and 80% of energy comes from this source. In 2018, 63.4 Mt of hard coal and 58.6 Mt of lignite coal were consumed in Poland for primary energy production, mostly by power plants (EURACOAL2020, Adu et al. 2020; Sówka et al. 2020). Hard coal deposits and most power plants are located in Upper Silesia and in the Lublin basin in the south of Poland. Lignite reserves at surface mines are located in central and south-west Poland. In 2018, the lignite mine located close to Bełchatów and Turów cities produced 54.3 million tons of lignite – 92.2% of the total lignite production in Poland. Research, especially for the area of Silesia region around coal power plants, confirms an additional anthropogenic share of  $^{238}\text{U}$  and  $^{210}\text{Po}$  isotopes in the atmosphere (Nowina-Konopko 1993). Specific activities of both isotopes in fraction  $<5\ \mu\text{m}$  of fly ashes were from 274.9 to 436.8 Bq/kg and from 153.9 to 1386 Bq/kg, respectively for  $^{238}\text{U}$  and  $^{210}\text{Po}$ . The annual maximum fallout in this region was

equal to  $25.7\ \text{Bq/m}^2$  and  $52.4\ \text{Bq/m}^2$ , respectively for  $^{238}\text{U}$  and  $^{210}\text{Po}$  ( $^{210}\text{Pb}$ ) (Nowina-Konopko 1993).

The high temperature industrial emission of  $^{210}\text{Pb}$  from Chinese facilities and biomass burning are estimated to be  $0.2\text{--}0.6\ \text{PBq/year}$  and  $1.6\ \text{PBq/year}$ , which accounts for about  $0.4\text{--}1.2\%$  and  $3\%$  of the  $^{210}\text{Pb}$  originating from  $^{222}\text{Rn}$  exhalation (Hirose et al. 2011, Sabuti et al. 2011, 2013). In Poland, the  $^{210}\text{Pb}$  contribution from high temperature processes has been estimated to be between 2.86 and 4.28% for conventional coal power plants (Długosz-Lisiecka 2015 b). These are rather minor contributions. Major contributions have been noted for  $^{210}\text{Po}$ . A previous study confirmed additional  $^{210}\text{Po}$  contributions of between 49 to even 91% (Długosz-Lisiecka 2019).

In this study, source apportionments of unsupported  $^{210}\text{Po}$  in the urban air are analyzed for the first time. The size distribution of unsupported  $^{210}\text{Po}$  and the migration of polonium contaminations on a regional and long-range scale are evaluated. As weather conditions have a significant impact on the dynamics of the transport of the air contaminations transport, temperature, humidity and wind velocity parameters were applied as weather indicators.

## Materials and methods

Samples were collected in the city center of Lodz, Poland. Two local hard coal power plants are located about 7 km (205 MW) and 11 km (200 MW) from the sampling point (Fig. 1). At a distance of 70 km from the sampling point there is a large lignite power plant (Central Poland) with a nominal electric power supply equal to 5100 MW (EURACOAL2020).

Aerosols were collected on dried and weighed glass fiber filters using a cascade impactor (TISH). A single acquisition session allowed six stages of particles with various sizes in different size fractions ( $<0.49\ \mu\text{m}$ ,  $0.49\text{--}0.95\ \mu\text{m}$ ,  $0.95\text{--}1.5\ \mu\text{m}$ ,  $1.5\text{--}3.0\ \mu\text{m}$ ,  $3.0\text{--}7.2\ \mu\text{m}$ ,  $>7.2\ \mu\text{m}$ ) to be collected.

The average sampling time for each sampling session was about 72 hours. In addition, during measurements, the exact amount of air passing through the filters was recorded. The filters were routinely dried in a laboratory drier at  $60^\circ\text{C}$  for 30–40 minutes and weighed to determine the mass of the



**Fig. 1.** Map of the interested region, (LP – lignite power plant-Belchatów city, CP3 – coal power plant Łódź city, CP4 – coal power plant Łódź city, SP – sampling point) (source: <http://openstreetmap.org.pl/>)

material. The filters were then ground and placed in beakers with 100 ml 1 M HCl on a magnetic stirrer, where they were mixed for about 30 minutes to wash the radionuclides from the surface of the aerosols. The solutions were then filtered through double paper filters to remove solid residues. The next step was the extraction of radionuclides from the HCl solutions with 5% triisooctylamine (TIOA) in xylene. Due to the better solubility of radionuclides in TIOA, they could be separated from other components in the solution. Each fraction was extracted twice with 5 ml TIOA in xylene (Długosz-Lisiecka and Bem 2020). The extracted radionuclide solutions were placed in scintillation vessels, to which 10 ml Ultima Gold F scintillator was added.

The next step was to measure sample activity using a liquid scintillation counter (LSC) with  $\alpha/\beta$  separation for the separate alpha emitter of  $^{210}\text{Po}$  and two beta emitters:  $^{210}\text{Pb}$  and  $^{210}\text{Bi}$ . For a proper activity analysis of individual  $^{210}\text{Pb}$ ,  $^{210}\text{Bi}$  and  $^{210}\text{Po}$  isotopes, the contaminations of other short-lived isotopes  $^{218}\text{Po}$ ,  $^{214}\text{Po}$ ,  $^{214}\text{Bi}$  and  $^{214}\text{Pb}$  were controlled, and their interference was reduced by delaying the measurement for about 24 hours.

In order to check the methodology and calculate the activity of  $^{210}\text{Pb}$ ,  $^{210}\text{Po}$  and  $^{210}\text{Bi}$  isotopes, certified reference material was tested in two concentrations containing an equilibrium portion of all three isotopes. The isotope recovery efficiency was determined by calibration based on the SRM 4337 standard. The chemical recovery of  $^{210}\text{Pb}$ ,  $^{210}\text{Bi}$  and  $^{210}\text{Po}$  isotopes was 97.7, 87.5 and 98.3%, respectively.

## Results

### Supported and unsupported $^{210}\text{Po}$ in the air

The decay products  $^{210}\text{Pb}$ ,  $^{210}\text{Bi}$  and  $^{210}\text{Po}$  of long-lived  $^{222}\text{Rn}$  are readily adsorbed on the surface of aerosol particles suspended in the air. The activities of  $^{210}\text{Bi}$  and  $^{210}\text{Po}$  grow during the residence time of aerosol particles in the air, while the activity of  $^{210}\text{Pb}$  does not change significantly due to its relatively long half-life of 22.3 years.  $^{210}\text{Po}$  may build up in the atmosphere, not only through the decay of  $^{222}\text{Rn}$ , but also as a result of industrial activities, especially those associated with high temperature processes.

In urban air, the two methods that calculate the aerosol residence time based on  $^{210}\text{Bi}/^{210}\text{Pb}$  and  $^{210}\text{Po}/^{210}\text{Pb}$  do not give

the same results for the same sample (Lozano et al. 2011, Długosz-Lisiecka 2016).

The isotopic fraction activity distribution is strongly dependent on the diameter of the aerosols. For  $^{210}\text{Pb}$ ,  $^{210}\text{Bi}$  and  $^{210}\text{Po}$ , the largest activities are associated with fractions with the smallest aerodynamic diameter of aerosols (Lozano et al. 2011, Vaasma et al. 2017). The mean aerosol residence time in the air depends on such processes as dry deposition, diffusion, sedimentation and wet deposition of the total aerosol fraction profile. As the diameter of aerosols decreases, their residence time increases. The calculated residence times based on the total aerosol profiles change seasonally as well as the method used to calculate them. Residence times calculated from the ratio of  $^{210}\text{Bi}/^{210}\text{Pb}$  in aerosol size profiles are in the range of 1 day to 16 days, while those calculated from the ratio of  $^{210}\text{Po}(\text{total})/^{210}\text{Pb}$  are significantly longer and range from 3 to 59 days.

In a previous study, the classic methods of assessing aerosol residence times were improved and allowed the relative contributions of different sources of  $^{210}\text{Po}$  radionuclide emissions into the urban air to be studied. This unique approach has been described in detail in the publications (Długosz-Lisiecka 2015 a, b) and summarized in the review article (Długosz-Lisiecka 2016).

The final equation is as follows:

$${}_{\text{un}}A_{\text{Po}} = \frac{A_{\text{Po}} - [A_{\text{Bi}} - A_{\text{Po}}]T_{\text{RC}}\lambda_{\text{Po}}}{1 + T_{\text{R}}\lambda_{\text{Po}}} \quad (2)$$

$$A_{\text{Po}} = {}_{\text{un}}A_{\text{Po}} + {}_{\text{sup}}A_{\text{Po}} \quad (3)$$

Where:

- $A_{\text{Po}}$  – unsupported polonium activity concentration ( $\mu\text{Bq}/\text{m}^3$ ),
- $A_{\text{Po}}$  – measured  $^{210}\text{Po}$  activity concentration in the air ( $\mu\text{Bq}/\text{m}^3$ ); the sum of supported and unsupported  $^{210}\text{Po}$  contributions,
- $A_{\text{Pb}}, A_{\text{Bi}}$  – measured  $^{210}\text{Pb}$  and  $^{210}\text{Bi}$  activity concentration, respectively ( $\mu\text{Bq}/\text{m}^3$ ),
- $\lambda_{\text{Po}}$  – decay constant of  $^{210}\text{Po}$  (1/day),
- $T_{\text{R}}$  – real aerosol residence time (day).

In this study, the activity size distribution of  $^{210}\text{Pb}$ ,  $^{210}\text{Bi}$ , supported  $^{210}\text{Po}$  and unsupported  $^{210}\text{Po}$  isotopes were monitored and used as a tool to identify anthropogenic  $^{210}\text{Po}$  sources.

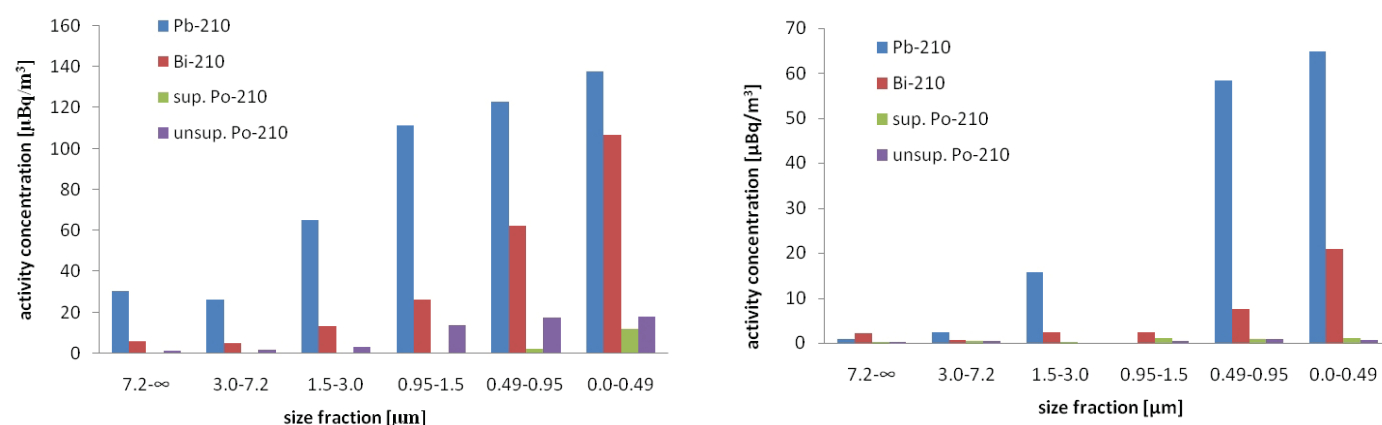


Fig. 2. Activity size distribution of  $^{210}\text{Pb}$ ,  $^{210}\text{Bi}$ , supported  $^{210}\text{Po}$  and unsupported  $^{210}\text{Po}$  isotopes a) December, 2019, b) June, 2019

Figure 1 shows the activity size distribution of  $^{210}\text{Pb}$ ,  $^{210}\text{Bi}$ , supported  $^{210}\text{Po}$  and unsupported  $^{210}\text{Po}$  isotopes in December and June 2019. In all fractions, the activity concentrations in winter were relatively higher than in summer. For comparison, the sum of activity concentrations for each month was calculated (Table 1).

The table shows that the contribution of unsupported  $^{210}\text{Po}$  ranged from  $2.3 \mu\text{Bq}/\text{m}^3$  in June to  $55.3 \mu\text{Bq}/\text{m}^3$  in December 2019. The contribution from supported  $^{210}\text{Po}$  ranged from  $1.7 \mu\text{Bq}/\text{m}^3$  in June to  $10 \mu\text{Bq}/\text{m}^3$  in December. Natural, supported  $^{210}\text{Po}$  isotope fluctuation results from  $^{222}\text{Rn}$  exhalation and  $^{210}\text{Pb}$  activity concentration in the surface air layer.  $^{210}\text{Pb}$  content in the air is not sensitive to artificial contribution, so its change should be rather correlated only with weather conditions and  $^{222}\text{Rn}$  exhalation.  $^{210}\text{Pb}$  activity concentration was higher in cold and wet seasons and lower in dry and hot months (Figure 1 and Table 1).

#### Method of determining the local and regional origins of $^{210}\text{Po}$ contaminations

The fate of radioactive aerosols containing supported and unsupported  $^{210}\text{Po}$  is associated with meteorological conditions. Three primary meteorological factors – temperature  $T$  ( $^{\circ}\text{C}$ ), wind velocity  $V$  (m/sec) and humidity  $H$  (%) – are the most important ones for the distribution of aerosols in the atmosphere

(Table 2). As these factors synergistically affect the dynamics of the atmosphere, one general meteorological parameter,  $Z$ , was developed for the needs of this study.  $Z$  is the function of temperature, wind velocity and humidity ( $Z=f(T, V, H)$ ), as shown in equation 4:

$$Z = \frac{T \cdot V}{H} \quad (4)$$

Temperature and humidity are naturally inversely correlated. A high temperature and strong winds are linked with an unstable, high – mixing atmosphere. The dry deposition velocity is a function of particle size and humidity. Parameter  $Z$  is intended to describe the atmospheric dynamics in a simple way. This parameter will only indicate general changes in the atmosphere in various (dry, warm, windy) seasons. The construction of this parameter should help with assessing the variability of the dynamics of radionuclide dispersion, including natural radioisotope concentration and radioactive contaminations.

Activity concentrations of  $^{210}\text{Pb}$  and  $^{210}\text{Bi}$  isotopes and supported and unsupported  $^{210}\text{Po}$  are shown in relation to parameter  $Z$  in Figures 3 and 4, respectively. A statistically significant ( $\alpha=0.05$ ) correlation was obtained for  $^{210}\text{Pb}$ ,  $^{210}\text{Bi}$  and supported  $^{210}\text{Po}$  activity concentrations:  $p=0.0005$ ,  $0.0009$  and  $0.007$ , respectively.

**Table 1.** Sum of  $^{210}\text{Pb}$ ,  $^{210}\text{Bi}$ , supported  $^{210}\text{Po}$ , and unsupported  $^{210}\text{Po}$  activities concentrations in fractionated aerosol profiles in various months (2019) ( $\mu\text{Bq}/\text{m}^3$ ) and  $T$  aerosol residence times based on  $^{210}\text{Bi}/^{210}\text{Pb}$  and sup.  $^{210}\text{Po}/^{210}\text{Pb}$  (days)

Month	Activity concentration ( $\mu\text{Bq}/\text{m}^3$ ) $^{210}\text{Pb}$	Activity concentration ( $\mu\text{Bq}/\text{m}^3$ ) $^{210}\text{Bi}$	Activity concentration ( $\mu\text{Bq}/\text{m}^3$ ) sup $^{210}\text{Po}$	Activity concentration ( $\mu\text{Bq}/\text{m}^3$ ) unsp $^{210}\text{Po}$	T(days) $^{210}\text{Bi}/^{210}\text{Pb}$	T(days) sup. $^{210}\text{Po}/^{210}\text{Pb}$
February	448±14	211±9	8.9	22.3	6.4	7.9
March	441±14	176±8	5.1	8.4	4.8	5.5
April	228±11	50±7	3.3	9.8	2.0	6.4
May	268±11	93±7	5.3	7.2	3.8	7.9
June	142±10	36±7	1.7	2.3	2.5	5.6
September	216±11	33±7	2.0	19.1	1.3	4.8
October	427±11	104±7	3.8	21.7	2.3	4.6
November	418±14	183±8	5.8	41.6	5.6	6.2
December	495±15	221±9	10.0	55.3	5.8	8.0

**Table 2.** Meteorological conditions:  $T(^{\circ}\text{C})$ ,  $H(\%)$ ,  $V(\text{m}/\text{sec})$  and parameter  $Z(^{\circ}\text{C m}/\text{sec} \%)$

Sampling month	$T(^{\circ}\text{C})$	$H(\%)$	$V(\text{m}/\text{sec})$	$Z(^{\circ}\text{C m}/\text{sec} \%)$
February	3.9	82.5	2.17	0.10
March	7.6	72.0	2.03	0.21
April	12.1	55.4	3.50	0.76
May	12.8	71.9	2.77	0.49
June	23.8	67.0	3.40	1.21
September	14.7	80.4	5.00	0.91
October	13.8	77.0	2.63	0.47
November	7.5	86.5	4.07	0.35
December	2.5	85.0	10.02	0.29

The activity concentration of unsupported  $^{210}\text{Po}$  in relation to parameter  $Z$  does not show any statistical correlation. This confirms the stochastic injection of higher unsupported  $^{210}\text{Po}$  portions into the urban air. However, parameter  $Z$  can change the activity concentrations of supported and local (close to the sampling point) unsupported  $^{210}\text{Po}$  in a similar way. Weather conditions, e.g. wind velocity in the city center, can dilute the concentration of  $^{210}\text{Po}$  regardless of its source.

Like the behavior of supported  $^{210}\text{Po}$ , the behavior of artificial  $^{210}\text{Po}$  in the lower troposphere emitted from local power plants (~ at a distance <10 km from the sampling point) is connected to weather, but only if the unsupported  $^{210}\text{Po}$  has a local origin. In the proposed method, it was assumed that parameter  $Z$  can be significantly correlated with the unsupported portions of  $^{210}\text{Po}$  from regional coal burning in

the air due to the fact that natural and artificial  $^{210}\text{Po}$  behave in a similar manner. Activity concentrations of unsupported  $^{210}\text{Po}$  from March, May and June show minimum values and a linear correlation with the  $Z$  parameter (Figure 4). Therefore, unsupported  $^{210}\text{Po}$  behaves the same as supported  $^{210}\text{Po}$ .

$$\text{local unsupported } ^{210}\text{Po} = -6.27 \cdot Z + 9.99 \quad (5)$$

Experimental equation (5) is true only for unsupported  $^{210}\text{Po}$  contamination in the air resulting from local  $^{210}\text{Po}$  pollution, e.g. from coal-fired power plants located close to the sampling point and working mostly for the electric power supply. In summer, long-range transport of  $^{210}\text{Po}$  contamination noticed at the sampling point is strongly reduced by a westerly wind. In this period, Lodz has not been

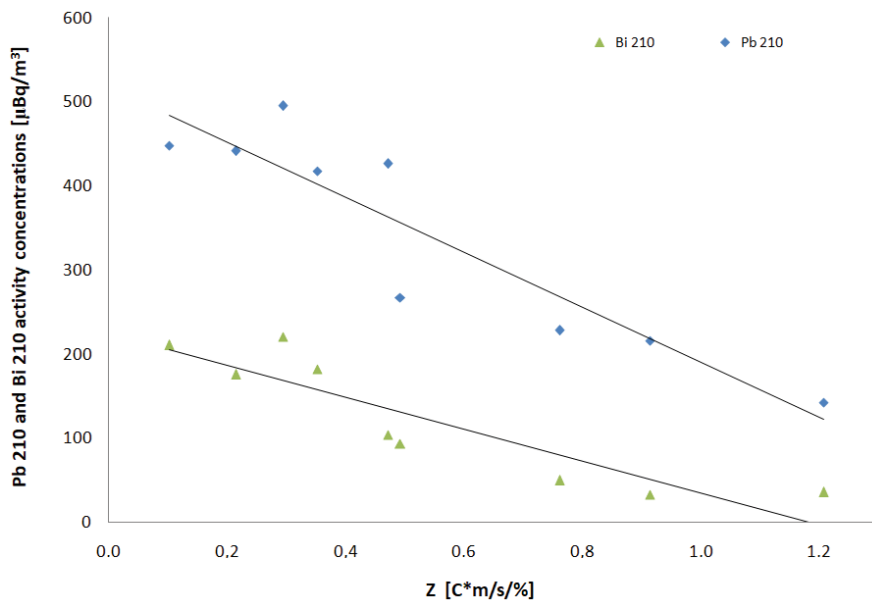


Fig. 3. Activity concentrations of  $^{210}\text{Pb}$ ,  $^{210}\text{Bi}$  isotopes in total fractionated aerosol profiles in relation to  $Z$  meteorological parameter  $Z$

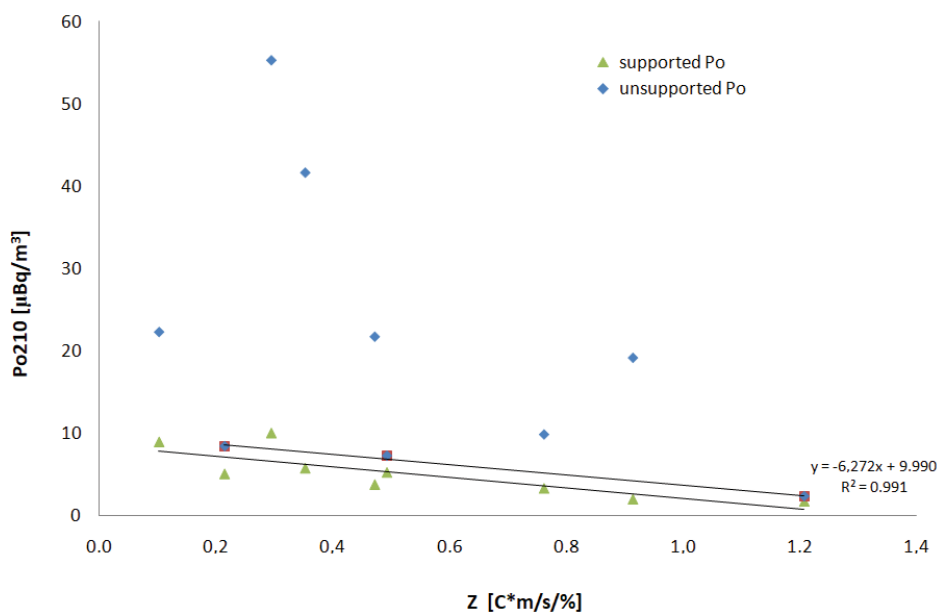


Fig. 4. Supported and unsupported  $^{210}\text{Po}$  activity concentrations in relation to meteorological parameter  $Z$

exposed to pollution from other regional power plants located at a distance  $\sim 100$  km.

$$Po_{\text{unSUP}} = Po_{\text{localunSUP}} + LR_{\text{unSUP}} Po \quad (6)$$

On the basis of equation 6, unsupported  $^{210}\text{Po}$  contamination is simply local unsupported  $^{210}\text{Po}$  portions and other portions, e.g. long-range unsupported  $^{210}\text{Po}$ , resulting from the long-range transport of contaminations.

A quantity estimation of local unsupported  $^{210}\text{Po}$  portions based on the Z parameter in equation 5 allows the quantity of the long-range  $^{210}\text{Po}$  contaminations from equation 6 to be estimated.

### Validation of the method

In the next step of our study, the methods used to determine the local and regional origins of contaminations were validated. In order to do this, aerosols were divided into two sections. The

first section contained coarse particles over  $1.5 \mu\text{m}$  in diameter (fractions 1, 2, and 3), and the second section contained fine particles from  $1.5$  to  $0.0 \mu\text{m}$  in diameter (fractions 4, 5 and 6).

Figure 5 shows the correlation between the sum of unsupported  $^{210}\text{Po}$  activity concentrations from section 1 (fraction no. 1, 2, 3) and local unsupported  $^{210}\text{Po}$  activity concentrations calculated directly from equation 5 for each month of 2019, based on the Z parameter.

A correlation coefficient calculated for the linear relationship,  $R = 0.82$  ( $R^2 = 0.70$ ), confirmed a statistically significant correlation.

Figure 5 shows a similar correlation between the sum of unsupported  $^{210}\text{Po}$  activity concentrations from fractions 4, 5 and 6 and long-range  $^{210}\text{Po}$  contribution. This time, the linear trend has the correlation coefficient  $R = 0.97$  ( $R^2 = 0.94$ ). This result confirms that long-range transport affects only fine particles with a diameter  $< 1.5 \mu\text{m}$ .

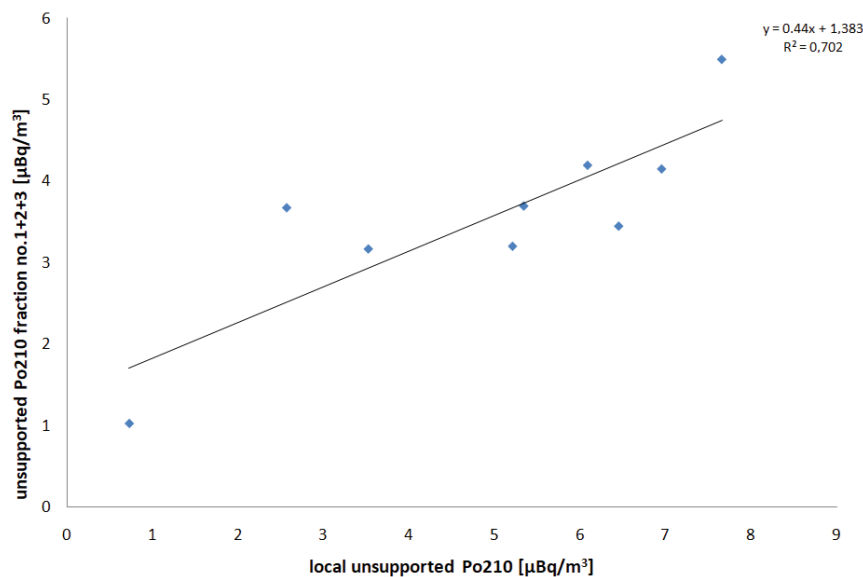


Fig. 5. Unsupported  $^{210}\text{Po}$  activity concentration from fractions 1, 2 and 3 as a function of local unsupported  $^{210}\text{Po}$

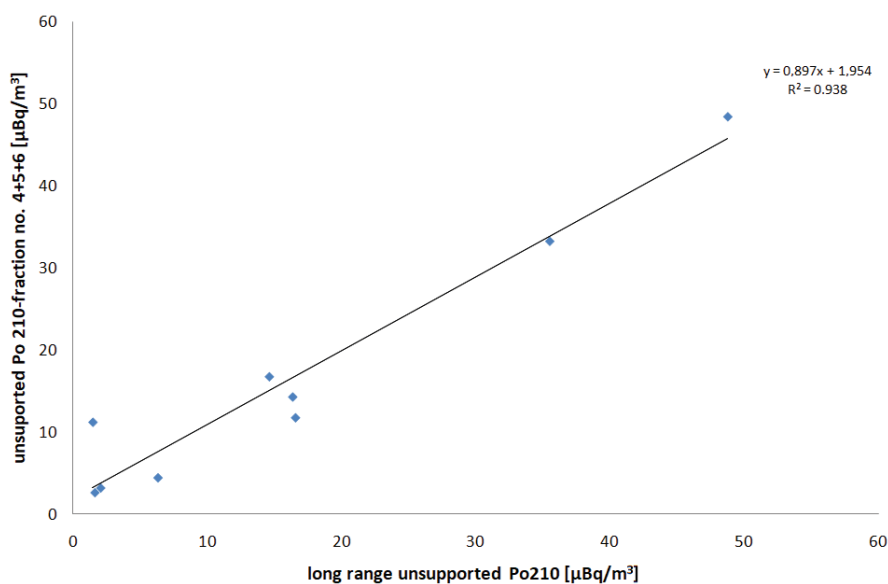


Fig. 6. Unsupported  $^{210}\text{Po}$  activity concentration from fractions 4, 5 and 6 as a function of long-range unsupported  $^{210}\text{Po}$  (long-range transport of  $^{210}\text{Po}$  contaminations)

Aerosol residence time depends on the particle size, atmospheric processes, and altitude in the atmosphere. Particles can be removed from the atmosphere by gravitational forces. Smaller dust particles fall more slowly and they can be removed with washing out processes from the atmosphere. In winter, this could be due to an additional anthropogenic inflow of dust from local and regional coal-fired power plants and domestic heating systems. The low quality of coal used is an additional problem.

However, during the summer, the coarse particles could have come from soil resuspension. Wind and lack of rainfall could lead to the increased contribution of this process. In summer, it was noticeable that the mass of particles in fraction 6 (0.0–0.49  $\mu\text{m}$ ) is significantly different to other seasons. When checking weather conditions of this season, it can be seen that the average wind speed was low and the average humidity was relatively high. Such conditions favor the persistence of the finest dusts in the atmosphere. During the summer months, it can also be seen that the proportion of particles in fraction 1, i.e. the particles with the largest aerodynamic diameter, increased.

## Conclusions

In this study  $^{210}\text{Pb}$ ,  $^{210}\text{Bi}$  and  $^{210}\text{Po}$  activity concentrations were measured in fractionated aerosols in six fractions. The impact of temperature, humidity, and wind velocity were analyzed using parameter Z, which was created for the purpose of this study. Supported and unsupported  $^{210}\text{Po}$  activity concentrations were calculated, and correlating them with parameter Z allowed local unsupported portions of  $^{210}\text{Po}$  and other sources of artificial  $^{210}\text{Po}$  emission, mostly linked with long-range transport, to be determined. This study also proposed an experimental equation for estimating local unsupported  $^{210}\text{Po}$ . This equation assumes that unsupported  $^{210}\text{Po}$  from local sources and supported  $^{210}\text{Po}$  produced from the gaseous  $^{222}\text{Rn}$  decay series behave in a similar way.

The proposed method for determining the local and regional origins of  $^{210}\text{Po}$  was validated using an independent approach based on the correlation of coarse aerosols (size  $d > 1.5 \mu\text{m}$ ; fraction 1, 2, and 3) with local unsupported  $^{210}\text{Po}$  activity concentrations, and the correlation of unsupported  $^{210}\text{Po}$  in fine aerosols (ranging from 0.0 to 1.5  $\mu\text{m}$  in diameter; fractions 4, 5 and 6) with unsupported  $^{210}\text{Po}$  activity concentrations from long-range transport. The high positive correlation ( $R^2 > 0.94$ ) (statistical significance  $p < 0.05$ ) of unsupported  $^{210}\text{Po}$  ( $\mu\text{Bq}/\text{m}^3$ ) with unsupported  $^{210}\text{Po}$  in the fine fraction ( $\mu\text{Bq}/\text{m}^3$ ) indicates an injection of additional unsupported  $^{210}\text{Po}$  from another source. This other source of artificial  $^{210}\text{Po}$  could be one of the biggest lignite power plants in Poland, located about 70 km from the sampling point.

In Poland, while there is a national system for monitoring the level of natural and artificial radioactivity in the atmosphere, industrialized areas are not routinely monitored. There are no restrictions on the emission of natural radionuclides in national legal regulations, which, even in large quantities, get into the environment.

## References

Aba, A., Ismael, A., Al-Boloushi, O., Al-Shammari, H., Al-Boloushi, A. & Malak, M. (2020). Atmospheric residence times and excess of unsupported  $^{210}\text{Po}$  in aerosol samples from the Kuwait Bay-

- Northern Gulf, *Chemosphere*, 261, pp. 127690, <https://doi.org/10.1016/j.chemosphere.2020.127690>.
- Adu, J. & Vellaisamy, M.V. (2020). Mathematical model development for non-point source in-stream pollutant transport, *Archives of Environmental Protection*, 46, 2, pp. 91–99
- Baskaran, M. (2011). Po-210 and Pb-210 as atmospheric tracers and global atmospheric Pb-210 fallout: a Review, *Journal of Environmental Radioactivity*, 102, pp. 500–513.
- Behbehani, M., Uddin, S. & Baskaran, M. (2020).  $^{210}\text{Po}$  concentration in different size fractions of aerosol likely contribution from industrial sources, *Journal of Environmental Radioactivity*, 222, 106323.
- Botezatu, E., Grecea, C. & Botezatu, G. (1996). Radiation exposure potential from coal-fired power plants in Romania Vienna, International Congress On Radiation Protection.
- EURACOAL, (2020). European Association for Coal and Lignite, Coal Industry across the Europe 7-th edition, ISSN 2034–5682.
- Filizok, I. & Gorgün, A.U. (2019). Atmospheric depositional characteristics of  $^{210}\text{Po}$ ,  $^{210}\text{Pb}$  and some trace elements in Izmir, Turkey, *Chemosphere*, 220, pp. 468–475.
- Hirose, K., Kikawada, Y., Doi, T. Su, C.C. & Yamamoto, M. (2011).  $^{210}\text{Pb}$  deposition in the Far East Asia: controlling factors of its spatial and temporal variations, *Journal of Environmental Radioactivity*, 102, pp. 514–519.
- Carvalho, F., Fernandes, S., Fesenko, S., Holm, E., Howard, B., Martin, P., Phaneuf, M., Porcelli, D., Pröhl, G. & Twining, J. (2017). The environmental behaviour of polonium technical reports series No. 484. International Atomic Energy Agency Vienna.
- Długosz-Lisiecka, M. & Bem, H. (2020). Seasonal fluctuation of activity size distribution of  $^7\text{Be}$ ,  $^{210}\text{Pb}$ , and  $^{210}\text{Po}$  radionuclides in urban aerosols, *Journal of Aerosol Science*, 144, 105544.
- Długosz-Lisiecka, M. (2016). The sources and fate of  $^{210}\text{Po}$  in the urban air: a review, *Environment International*, 94, pp. 325–330.
- Długosz-Lisiecka, M. (2019). Chemometric methods for source apportionment of  $^{210}\text{Pb}$ ,  $^{210}\text{Bi}$  and  $^{210}\text{Po}$  for 10 years of urban air radioactivity monitoring in Lodz city, Poland, *Chemosphere*, 220, pp. 163–168.
- Długosz-Lisiecka, M. (2015). Excess of Polonium-210 activity in the surface urban atmosphere, Part 1, Fluctuation of the  $^{210}\text{Po}$  excess in the air, *Environ. Sci.: Processes Impacts*, 17(2), pp. 458–464, a.
- Długosz-Lisiecka, M. (2015). Excess of Polonium-210 activity in the surface urban atmosphere. Part 2. Origin of  $^{210}\text{Po}$  excess, *Environ. Sci.: Processes Impacts*, 17(2), pp. 465–470, b.
- Ioannidou, A., Eleftheriadis, K., Gini, M., Gini, L., Manenti, S. & Groppi, F. (2019). Activity size distribution of radioactive nuclide  $^7\text{Be}$  at different locations and under different meteorological conditions, *Atmospheric Environment*, 212, pp. 272–280.
- Kaynar, S.Ç., Kaynar, U.H., Hiçsönmez, Ü. & Sevinç, O.Ü. (2018). Determination of  $^{210}\text{Po}$  and  $^{210}\text{Pb}$  depositions in lichen and soil samples collected from Köprübaşı-Manisa, Turkey, *Nuclear Science and Techniques*, 29, 10, 1007/s41365-018-0428-7.
- Lozano, R.L., San Miguel, E.G. & Bolívar, J.P. (2011). Assessment of the influence of in situ  $^{210}\text{Bi}$  in the calculation of in situ  $^{210}\text{Po}$  in air aerosols: Implications on residence time calculations using  $^{210}\text{Po}/^{210}\text{Pb}$  activity ratios, *Journal of Geophysical Research*, 116, D08206, DOI: 10.1029/2010JD014915.
- Mertens, J., Lepaumier, H., Rogiers, P., Desagher, D., Goossens, L., Duterque, A., Le Cadre, E., Zarea, M. & Blondeau, J. (2020). Webber M., Fine and ultrafine particle number and size measurements from industrial combustion processes: Primary emissions field data, *Atmospheric Pollution Research*, 11, 4, pp. 803–814.
- Marley, N.A., Gaffney, J.S., Drayton, P.J., Mary, M. Cunningham, K. Orlandini, A. & Paode, R. (2000). Measurement of  $^{210}\text{Pb}$ ,  $^{210}\text{Po}$  and  $^{210}\text{Bi}$  in Size-Fractionated Atmospheric Aerosols: An

- Estimate of Fine-Aerosol Residence Times, *Aerosol Science and Technology* 32, pp. 569–583.
- Nowina-Konopka, M. (1993). Radiological hazard from coal-fired power plants in Poland. *Radiat. Prot. Dosim.* 46 (3), pp. 171–180.
- Nelson A.W., Eitheim, E.S., Knight, A.W., May, D. & Schultz, M.K. (2017). Polonium-210 accumulates in a lake receiving coal mine discharges – anthropogenic or natural? *Journal of Environmental Radioactivity*, 167, 211–221.
- Ozden, B., Guler, E., Vaasma, T., Horvath, M., Kiisk, M. & Kovacs, T. (2017). Enrichment of naturally occurring radionuclides and trace elements in Yatagan and Yenikoy coal-fired thermal power plants. Turkey, *Journal of Environmental Radioactivity*, 188, pp. 100–107.
- Ozden, B., Vaasma, T., Kiisk, M. & Tkaczyk, A.H. (2016). A modified method for the sequential determination of  $^{210}\text{Po}$  and  $^{210}\text{Pb}$  in Ca-rich material using liquid scintillation counting, *Journal of Radioanalytical and Nuclear Chemistry*, 311 (1), pp. 365–373.
- Ouyang, J., Song, L.-J., Ma, L.-L., Luo, M. & Xu, D.-D. (2018). Temporal variations, sources and tracer significance of Polonium-210 in the metropolitan atmosphere of Beijing, China, *Atmospheric Environment*, 193, 2018, pp. 214–223.
- Pham, M.K., Betti, M., Nies, H. & Povinec, P. (2011). Temporal changes of  $^7\text{Be}$ ,  $^{137}\text{Cs}$  and  $^{210}\text{Pb}$  activity concentrations in surface air at Monaco and their correlation with meteorological parameters, *Journal of Environmental Radioactivity*, 102, 11, pp. 1045–1054.
- Poluszyńska J. (2020). The content of heavy metal ions in ash from waste incinerated in domestic furnaces, *Archives of Environmental Protection*, 46, 2, pp. 68–73.
- Sabuti, A.A. & Mohamed, C.A.R. (2011). Natural Radioisotopes of Pb, Bi and Po in the Atmosphere of Coal Burning Area, *Environment Asia*, 4, pp. 49–62, 10,14456/ea,2011,18.
- Sabuti, A.A. & Mohamed, C.A.R. (2013). Residence time of Pb-210, Bi-210 and Po-210 in the atmosphere around a coal-fired power plant, Kapar, Selangor, Malaysia, *Pollution Research*, 32, pp. 907–915.
- Sówka I., Badura M., Pawnuik M., Szymański P. & Batog P. (2020). The use of the GIS tools in the analysis of air quality on the selected University campus in Poland. *Archives of Environmental Protection*, 46, 1, pp. 100–106
- Sýkora, I. & Povinec, P.P. (2020). Natural and anthropogenic radionuclides on aerosols in Bratislava air, *Journal of Radioanalytical and Nuclear Chemistry*, 325, pp. 245–252, <https://doi.org/10.1007/s10967-020-07219-0>.
- Szaciłowski, G., Ośko, J. & Pliszczyński, T. (2019). Determination of  $^{210}\text{Po}$  in air filters from metallurgic industry, *Journal of Radioanalytical and Nuclear Chemistry*, 322, pp. 1351–1356, <https://doi.org/10.1007/s10967-019-06858-2>.
- Vaasma, T., Loosaar, J., Gyakwaa, F., Kiisk, M., Özden, B. & Tkaczyk, A.H. (2017). Pb-210 and Po-210 atmospheric releases via fly ash from oil shale-fired power plants, *Environmental Pollution*, 222, 210–218.
- Vecchi, R., Piziali, F.A., Valli, G., Favaron, M. & Bernardoni, V. (2019). Radon-based estimates of equivalent mixing layer heights: A long-term assessment. *Atmospheric Environment*, 197, pp. 150–158.
- Wasielewski R., Wojtaszek M. & Plis A. (2020). Investigation of fly ash from co-combustion of alternative fuel (SRF) with hard coal in a stoker boiler. *Archives of Environmental Protection*. 46, 2, pp. 58–67.
- Yan G., Cho H.-M., Lee, I. & Kim, G. (2012). Significant emissions of  $^{210}\text{Po}$  by coal burning into the urban atmosphere of Seoul, Korea, *Atmospheric Environment*, 54, 80–85.

## Ocena udziałów zanieczyszczeń antropogenicznego izotopu Po-210 w powietrzu atmosferycznym

**Streszczenie:** W pracy dokonano podziału źródeł dodatkowych porcji izotopu Po-210. Rozkłady wielkości frakcji zarówno związanej, jak i niezwiązanej Po-210 w aerozolach miejskich mierzono od lutego do grudnia 2019 r. Wyniki potwierdziły, że aktywność Po-210 w atmosferze jest istotnie zwiększona przez dopływ dodatkowych porcji Po-210 związanych z uwalnianiem produktów spalania węgla, zwłaszcza w okresie zimowym. Próbkę pobierano w centrum Łodzi, w Polsce. Dwie lokalne elektrownie opalane węglem kamiennym znajdują się około 7 km (205 MW) i 11 km (200 MW) od punktu poboru próbek. W odległości 70 km od punktu poboru próbek znajduje się duża elektrownia na węgiel brunatny (Elektrownia Bełchatów) o mocy 5100 MW. Aerozole zbierano na filtrach z włókna szklanego za pomocą impaktora kaskadowego (TISH). Produkty rozpadu radonu -222, tj. Pb-210, Bi-210 i Po-210 są łatwo adsorbowane na powierzchni cząstek aerozolu zawieszonych w powietrzu i chociaż aktywność  $^{210}\text{Pb}$  nie zmienia się znacząco ze względu na stosunkowo długi okres półtrwania wynoszący 22,3 lat, to aktywności Bi-210 i Po-210 przyrastają w czasie przebywania cząstek aerozolu w powietrzu. Temperaturę, wilgotność i prędkość wiatru analizowano wspólnie za pomocą parametru Z, który został zdefiniowany na potrzeby niniejszych badań. Obliczono związane i niezwiązane stężenia aktywności Po-210, a skorelowanie ich z parametrem Z pozwoliło określić ilościowo udział źródeł lokalnej dodatkowej porcji Po-210 i innych źródeł dodatkowej, antropogenicznej emisji Po-210, związanej z transportem dalekiego zasięgu.